

Department of Physics and Astronomy
Heidelberg University

Bachelor Thesis in Physics
submitted by

Tobias Thaller

born in Gmund am Tegernsee (Germany)

2024

Exploring Polarization-Splitting Grating Couplers on a Silicon-Nitride platform at 1550 nm

This Bachelor Thesis has been carried out by Tobias Thaller at the
Kirchhoff Institute in Heidelberg
under the supervision of
Liam McRae

Abstract

As nanoscale fabrication techniques advanced, photonic integrated circuits gained popularity for their speed and energy efficiency. A major challenge involves the coupling between fiber and nano-optical devices. A promising solution to this is the use of grating couplers, which can orthogonally couple light at any location on a chip. While already firmly established on the SOI platform, they have also become essential on low-index platforms such as SiN in recent years. This relatively new material platform is characterized by its low propagation losses and exceptional power handling capabilities, making it attractive for a wide range of applications. While standard grating couplers efficiently couple light of only one polarization, polarization-splitting grating couplers can couple light regardless of its polarization. The latter have not yet been realized on the SiN platform, making their investigation particularly worthwhile. This thesis determines optimal parameters for a 2D grating coupler design on SiN using FDTD simulations. The simulated maximal coupling efficiency is 51.8%, without employing any additional back reflector. Furthermore, the development of polarization-splitting grating couplers on SiN is explored, with 3D simulations indicating that such an endeavor is achievable.

Zusammenfassung

Einhergehend mit dem schnellen Fortschritt von Fertigungstechniken haben photonenintegrierte Schaltkreise aufgrund ihrer Geschwindigkeit und Energieeffizienz an Popularität gewonnen. Eine vielversprechende Lösung für die Kopplung zwischen Chip und Faser ist der Einsatz von Grating-Couplern, die Licht orthogonal an jede Stelle auf der Oberfläche eines Chips koppeln können. Während sie auf der SOI-Plattform bereits fest etabliert sind, sind sie auch auf Plattformen mit niedrigem Brechungsindex wie SiN unverzichtbar geworden. Diese relativ neue Materialplattform zeichnet sich durch ihre geringen Ausbreitungsverluste und durch außergewöhnliche Belastbarkeit aus, was sie für eine breite Palette von Anwendungen attraktiv macht. Während herkömmliche Grating-Coupler nur Licht einer speziellen Polarisation effizient koppeln können, sind polarisationsteilende Grating Coupler unabhängig von der Polarisation des einfallenden Lichts. Letztere wurden bisher noch nicht auf der SiN-Plattform realisiert, was ihre Untersuchung besonders lohnenswert macht. Diese Arbeit bestimmt optimale Parameter für ein 2D-Grating-Coupler-Design auf SiN unter Verwendung von FDTD-Simulationen. Die simulierte maximale Kopplungseffizienz beträgt 51.8%, ohne dass dabei ein zusätzlicher Rückreflektor eingesetzt wurde. Darüber hinaus wird die Entwicklung von polarisationsteilenden Grating-Couplern auf SiN untersucht, wobei 3D-Simulationen darauf hindeuten, dass ein solches Unterfangen erreichbar ist.

Contents

1	Introduction	1
2	Theoretical background	3
2.1	Snell's law and Gaussian dispersion	3
2.2	Modes and effective index	3
2.3	Polarization	4
2.4	Grating couplers & bragg equation	4
2.5	Polarization splitting grating coupler	6
3	Simulation procedure	11
3.1	Simulation software Ansys Lumerical	11
3.2	SiN Material Stack	12
3.3	Finding optimal parameters for a 2D grating coupler	13
3.3.1	Out-coupling simulation configuration	14
3.3.2	In-coupling simulation configuration	17
3.4	Optimizing mesh values	19
3.5	Continuation in 3D	20
4	Outlook	21
4.1	Improvement of the 2D GC	21
4.2	Next steps	23
5	Conclusion	25
	Appendices	28

1 Introduction

As fabrication methods have advanced, the range of applications for photonic integrated circuits (PICs) has broadened, now including major industry fields like quantum technologies [1] and artificial intelligence [2–4]. This thesis is based upon SiN as a material platform, mainly because of its relatively good manufacturability and its low loss waveguides ($< 1 \text{ dB m}^{-1}$) that can handle high optical power [5, 6].

To fully exploit the advantages of SiN devices, an efficient fiber-to-chip interface is crucial. The strategies to date can be divided into two categories: edge couplers, which direct light to the chip’s facet and subsequently in-plane into the optical fiber and vertical couplers, which couple to fiber array units placed atop the chip. In many cases the latter ones are preferred as they generally work with standard single-mode fibers [7] and most of all due to their ability of orthogonal light coupling to the chip surface at any location within the chip area. This feature is especially critical for the development of large-scale prototypes in densely integrated photonic circuits, which becomes increasingly important as the complexity of PICs grows.

The most popular vertical couplers are grating couplers (GCs) which are introduced in Section 2.4. One of the biggest challenges to realize them on the SiN platform is the relatively low grating strength (which describes how much power gets diffracted out of the waveguide per distance) due to the low index contrast ($\Delta n \approx 0.56$ at $\Lambda = 1550 \text{ nm}$). As a consequence, the grating region has to be longer than $40 \mu\text{m}$ [8] (compare to Section 3.3), which is significantly bigger than the mode-field diameter of conventional optical fibers ($\approx 10 \mu\text{m}$). To effectively couple light between the WG and the fiber, their mode mismatch has to be dealt with in both, longitudinal (direction of gratings) and transverse directions. One possibility for mode-matching in longitudinal direction despite this long grating region is the self-imaging effect of linear apodized gratings while using a negative diffraction angle, which has been demonstrated in [9] and will be explained in more detail in Section 3.3. As shown in [10], linear apodization nicely approximates the optimal apodization to achieve gauss-like up-reflection. The focusing effect in transverse direction can be achieved using circular gratings, as demonstrated in [11]. Section 2.4 will go into more detail. Using standard optical fibers and the just mentioned techniques for mode-matching between the WG and the fiber, a coupling efficiency of -0.55 dB at $\lambda = 1550 \text{ nm}$ has been achieved on the SiN platform [12], making it comparable to silicon-on-insulator grating couplers [13–15].

The main drawback of this setup is that it is designed for one specific polarization state of the Gaussian beam in the fiber while the coupling efficiency is strongly polarization sensitive [10], which will also be shown in this thesis. Controlling the polarization state of fibers can be difficult, especially for setups where several hundred fibers have to be coupled on one device. Having to add polarization controllers, the increase in components may also result in efficiency problems in certain setups. An elegant solution for this problem are polarization-splitting grating couplers (PSGCs), which have mainly been realized on the SOI platform so far [16–20].

This thesis investigates the implementation of a PSGC on the SiN platform, leveraging concepts of focusing diffractive gratings as discussed in [12]. In contrast to that study, this thesis utilizes an in-coupling configuration to optimize coupling efficiency, making it easier to observe and optimize the region between the gratings and the WG during simulations.

2 Theoretical background

This chapter establishes the theoretical foundations of this thesis, spanning from concepts of fundamental optoelectronics to specific mathematical derivations needed for the grating coupler design discussed in the chapter following this one.

2.1 Snell's law and Gaussian dispersion

Snell's law describes how light behaves at the transition between two materials of different refractive index, which will be crucial in later sections of this thesis. It establishes a relationship between the angle of incidence (θ_1) and angle of refraction (θ_2) at the border of the material 1, where the beam comes from with the refractive index n_1 , and the material 2, in which the beam gets diffracted and has a refractive index n_2 :

$$\frac{\sin \theta_1}{\sin \theta_2} = \frac{n_2}{n_1} \quad (2.1)$$

A Gaussian beam refers to a type of electromagnetic wave where the electric field amplitude distribution in any cross-sectional plane perpendicular to the direction of propagation is given by a Gaussian function. It is particularly relevant in Optoelectronics. The beam's radius $\omega(z)$ increases with the distance from its waist z (the position where the beam's radius is the smallest):

$$\omega(z) = \sqrt{1 + \left(\frac{\lambda \cdot z}{\pi \omega_0^2 n}\right)^2} \quad (2.2)$$

λ is the wavelength, ω_0 is the radius at the waist and n is the refractive index of the medium.

2.2 Modes and effective index

In PICs, modes refer to the distinct patterns of electromagnetic fields that can propagate through the waveguides formed on the PIC. These modes are solutions to Maxwell's equations under the boundary conditions imposed by the waveguide's geometry and material properties. Light confined in a waveguide can travel in different modes, each with a specific spatial distribution of the electric and magnetic fields. Single-mode waveguides

support only one mode, while multimode waveguides can support several modes. The propagation velocity of a mode is determined by its effective refractive index, which is defined by the waveguide's refractive index profile (for further details, take a look at [21]). Therefore, modes are critical in determining the behavior and performance of PIC components like modulators, switches or couplers.

2.3 Polarization

Polarization of electromagnetic waves refers to the orientation of the electric field vector. In the domain of PICs, controlling polarization is crucial, since the interaction of light with PIC elements often depends on this orientation. Components within PICs are designed to guide, manipulate, and exploit these polarization states for improved functionality in applications like optical data transmission and processing. Proper management of polarization is critical for minimizing losses and other impairments in signal integrity, leading to more efficient and higher-performing photonic systems.

2.4 Grating couplers & bragg equation

A grating coupler (GC) is a periodic structure, which uses the concept of diffraction and constructive interference to couple light from a fiber to a waveguide or the other way round. As grating couplers can be modeled as linear open systems, the reciprocity theorem is valid, which means that the coupling efficiency for the out-coupling (source in the waveguide as shown in Figure 2.2a) and in-coupling (source in the fiber above the chip) configuration has to be the same [22]. The change of refractive index due to the alternation of two materials causes the incoming beam to partly get diffracted out of the waveguide as refractive index change occurs. Only in the direction where this diffracted light interferes constructively, beams of light will be visible. The conditions for constructive interference are easier to understand looking at the out-coupling configuration. Therefore, Figure 2.1 is used to illustrate the Bragg equation for gratings [9]:

$$n_{eff} \cdot \Lambda - n_c \cdot \Lambda \cdot \sin(\theta) = \lambda \cdot m = \lambda \quad (2.3)$$

For constructive interference, the phase of the diffracted beam in point A and point B has to be the same. As a consequence, the sum of the period Λ weighted by the effective index of the gratings n_{eff} and the length l weighted by the effective index of the cladding n_c has to be an integer multiple ($m \in \mathbb{N}$) of the wavelength λ . We directly set $m = 1$ as we are only interested in the first diffraction order, mainly because this is the most

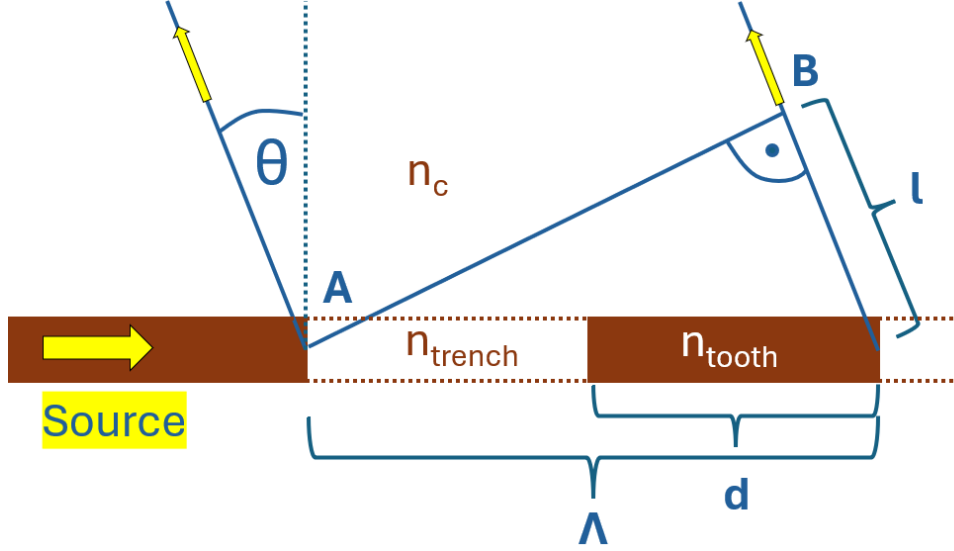


Fig. 2.1 Schematic of the beginning of the gratings. The light originating from the source gets diffracted at the negative diffraction angle θ . The period of the grating is indicated by Λ and the tooth-length by d .

efficient in terms of the energy distribution. The length l is given as $l = \sin \theta \cdot \lambda$ and n_{eff} , the effective refractive index of the light in the grating structure can (as a first-order approximation) be expressed as a weighted average of n_{tooth} , the effective index of the unetched SiN-tooth, and n_{trench} , the effective index of the etched SiO₂-trench [9]:

$$n_{eff} = FF \cdot n_{tooth} + (1 - FF) \cdot n_{trench} \quad (2.4)$$

The weight is called the filling factor FF and given by $FF = \frac{d}{\Lambda}$ where d is the length of the tooth as shown in Figure 2.1. The negative sign in Equation 2.3 is due to the diffraction angle θ being negative, indicating that the diffracted beam inclines towards the source, as it can be seen in Figure 2.1 as well. Consequently, $\sin \theta$ is negative, neutralizing the negative sign of Equation 2.3. Given that future calculations are based on this equation, treating the diffraction angle consistently as being negative is essential.

In the case of a constant grating, the period and filling factor stays the same over the length of all gratings. In general, both of these two parameters can be varied to tailor the properties of the grating coupler. This is called apodization. Practically, the period is often kept constant to guarantee constructive interference, while only the filling factor is varied.

Figure 2.2a shows a linear apodized grating (with constant period). The negative diffraction angle increases with a growing filling factor, as the condition of Equation 2.3 for constructive interference has to stay fulfilled. Thus, if the initial filling factor is chosen to

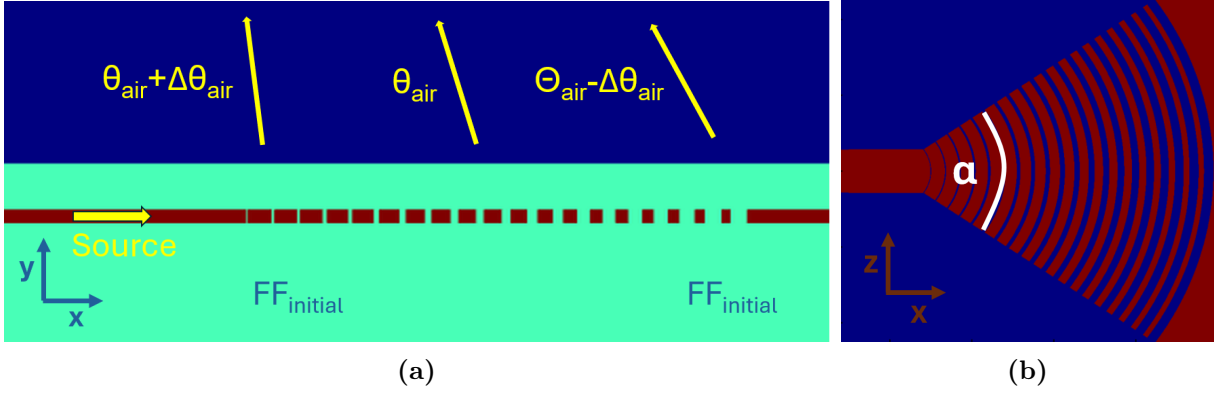


Fig. 2.2 a: out-coupling design of a grating coupler with 20 gratings. SiO₂ is shown in green, SiN in red, and air in blue. The lower the filling factor, the smaller is the diffraction angle.

b: curved gratings with opening angle α . In this plot, taken by an index monitor, the blue color corresponds to SiO₂.

be bigger than the final filling factor, the upward reflected beam converges at a specific distance away from the chip (as indicated in Figure 2.2a). This is called the self-imaging effect and can be used to effectively couple light with a GC even if the length of the coupler has to be significantly bigger than the mode-field diameter of the fiber in which the light has to couple (which is the case on the SiN platform due to its low index contrast).

Mode-matching the fiber in transverse direction with the much smaller waveguide can be achieved with curved gratings. The optimal shapes for the gratings are ellipse-like curves as can be calculated using the bragg equation [10]. Only for a vanishing diffraction angle ($\theta = 0$) the ellipses become circles (compare to Figure 2.2b), which are normally used for focusing gratings as they approximate well the optimal shape for small diffraction and opening angles.

2.5 Polarization splitting grating coupler

As GCs are very polarization sensitive [10], an alignment of the polarization of the incoming light with the WG mode into which the light is intended to couple is necessary to ensure efficient mode matching in order to achieve a high coupling efficiency. For most GC designs like the one used in [12], on which this work is based, this means that only transverse electric (TE) polarized light can effectively couple into the waveguide. This drawback is addressed with a PSGC, which is able to efficiently couple light to a waveguide regardless of its polarization when coming out of the fiber.

A PSGC consists of two GCs placed on top of each other at a 90-degree angle, as shown in Figure 2.3. The injecting source is rotated by 45 degrees to align with the PSGC's axis of

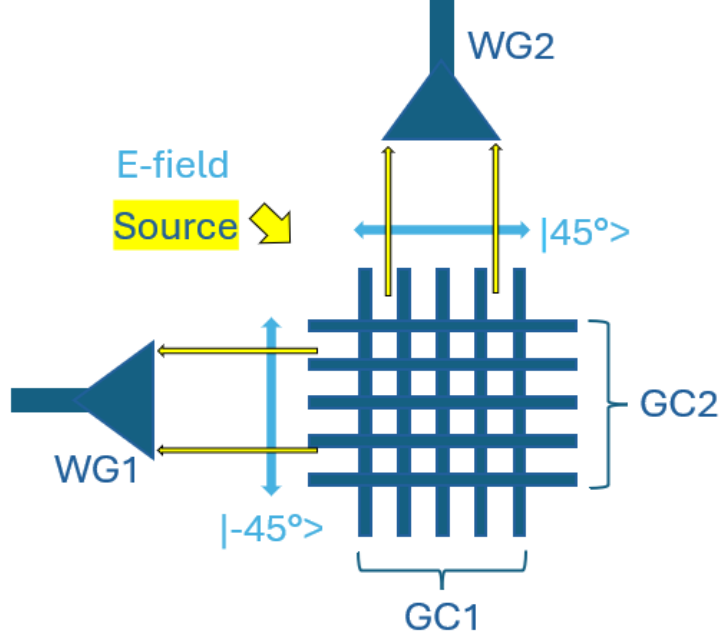


Fig. 2.3 Illustration of the working principle of a PSGC. GC1 couples to WG1 if the polarization angle from the source is 45° . If it is -45° , only GC2 couples to WG2. The triangle-like shapes at the beginning of the WGs are tapers to confine the light in transverse direction. The light blue arrows indicate the direction of the E-field and therefore the polarization of the beam from the source. The source illuminates the PSGC from above while featuring a deviation from the normal to the PSGC of the diffraction angle. It is this perspective that makes the yellow arrow so short.

symmetry. Each of the two GCs can effectively couple one polarization into the respective WG, with the two polarizations being orthogonal to each other. If the polarization of the out-coming beam of the fiber is at state $|-45^\circ\rangle$ the beam couples into waveguide 1. If it is at state $|45^\circ\rangle$, it couples into WG 2. All other polarizations, which can be expressed as a superposition of these two states, couple partly in WG 1 and partly in WG 2. If both GCs are identical, the coupling efficiency is independent of the polarization. Note that the polarization after the coupling process is the same (E-field in the direction of the surface of the chip) in both waveguides, so that the PSGC can be used for polarization diversity configurations [23].

For a GC where the injecting source is rotated by $\phi = 45^\circ$ around the normal to the chip, like it is shown in Figure 2.4b, the bragg Equation 2.3 has to be slightly adopted:

$$\begin{aligned}
 n_{eff} \cdot \Lambda - n_c \cdot \Lambda \cdot \sin(\beta - 90^\circ) &= \lambda \\
 n_{eff} \cdot \Lambda + n_c \cdot \Lambda \cdot \sin(90^\circ - \beta) &= \lambda \\
 n_{eff} \cdot \Lambda + n_c \cdot \Lambda \cdot \cos(\beta) &= \lambda
 \end{aligned} \tag{2.5}$$

Note: β is positive in this definition in contrast with the negative diffraction angle $\beta - 90^\circ$!

The only difference between Equation 2.3 and 2.5 is, that $l = -\sin(\theta)\Lambda$ has to be replaced with $\tilde{l} := -\sin(\beta - 90^\circ)\Lambda = \cos(\beta)\Lambda$, which can be understood remembering Figure 2.1 of the preceding section and looking at Figure 2.4a. Like l is aligned with the source at $\phi = 0^\circ$, \tilde{l} is the equivalent of l , but aligned with the source at $\phi = 45^\circ$.

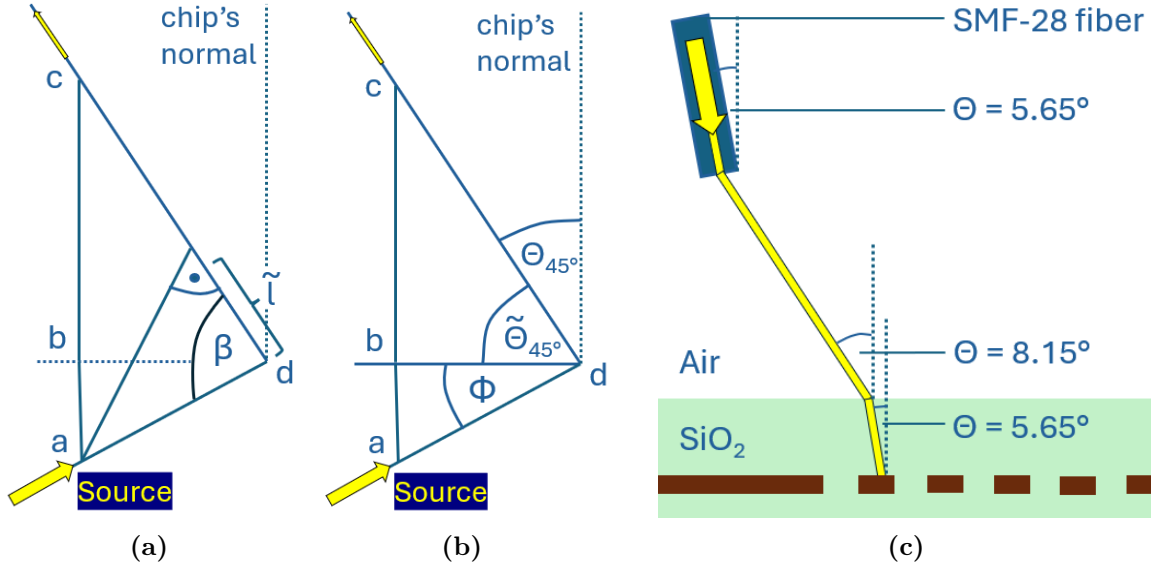


Fig. 2.4 a, b: Both figures represent the identical setup while only different angles are indicated. They show an illustration of an in-coupling setup where the injection axis (defined by the line \overline{ca}) is rotated 45° out of the plane defined by the chip's normal and the direction of the gratings (defined by the line \overline{ad}). The gratings are situated in the plane defined by the points a, d and b, but they are not included in the drawing.
c: Snells law applied two times to the in-coupling setup.

As we want the PSGC to match the 8° polishing angle of our in-house fiber array, we set $\theta_{45^\circ} = -8^\circ$, which is the diffraction angle or angle of incidence, defined as the angle between the incident beam and the normal to the surface of the chip as is shown in Figure 2.4b. $\theta := \theta_{0^\circ}$ represents the diffraction angle for $\phi = 0^\circ$, where the source is situated on the plane defined by the chip's normal and the gratings' symmetry axis. Optimizing parameters for a $\phi = 0^\circ$ setup is relatively simple because this can be achieved using 2D simulations, as described in Section 3.3. To guarantee that the parameters determined in this step are also applicable to the PSGC design, where 3D simulations are essential, it is necessary to ensure that the values for n_{eff} and Λ are identical in both the Bragg Equations (2.3 and 2.5). As n_c and λ are constants in this setup, these two equations can be subtracted from one another and the following equality is obtained:

$$\sin(\theta) = -\cos(\beta) \quad (2.6)$$

β is uniquely defined by θ_{45° , ϕ as can be seen from Figures 2.4a and 2.4b. Appendix 1 shows how these figures can be used to derive the corresponding equation:

$$\cos \beta = \cos \tilde{\theta}_{45^\circ} \cdot \cos \phi \quad (2.7)$$

Combining Equation 2.6 and 2.7 establishes the following relationship:

$$\sin(\theta) = -\cos \tilde{\theta}_{45^\circ} \cdot \cos \phi \quad (2.8)$$

This makes it possible to calculate the diffraction angle θ for which n_{eff} and Λ of Equation 2.3 have to be optimized in order to find the optimal values for the two grating couplers making up a PSCG which has a diffraction angle of -8° at its symmetry axis. Plugging in the two given values $\theta_{45^\circ} = -8^\circ$ and $\phi = 45^\circ$ into Equation 2.8 results in the following value for the diffraction angle, which will be used for the simulations of the following chapter:

$$\theta = -\arcsin\left(\cos \tilde{\theta}_{45^\circ} \cdot \cos \phi\right) \approx -5.65^\circ \quad (2.9)$$

$\theta_{45^\circ} = -8^\circ$ is the angle of the beam propagating through the fiber. In our case, it is a SMF-28 single-mode fiber, which has a core that has a refractive index of $n \approx 1.44$ similar to the cladding material SiO_2 . In between the fiber and the cladding, the beam is propagating in air and therefore is refracted two times before reaching the gratings. At the transition from SiO_2 ($n_{\text{SiO}_2} = 1.44$) to air ($n_{\text{air}} = 1$), the angle of incidence (which is the angle of the beam with the normal to the chip) is getting bigger because of Snell's law (compare to Equation 2.1). At the second transition from air to SiO_2 , this increase is reversed so that the angle of incidence in the cladding is the same as in the fiber. This is illustrated in Figure 2.4c for a fiber angle of $\theta_{\text{SiO}_2} = 5.65^\circ$ corresponding to the diffraction angle calculated just above. Applying the Equation 2.1 of Snell's law returns the following θ_{air} , the angle of incidence in air for this setup:

$$\theta_{\text{air}} = \arcsin\left(\sin(\theta_{\text{SiO}_2}) \cdot \frac{1.44}{1}\right) \approx 8.15^\circ \quad (2.10)$$

This is the angle at which the source must be positioned over the chip in the in-coupling configuration for the 2D simulations discussed in the next chapter.

3 Simulation procedure

Fabrication of Nanostructures like PICs on the SiN platform is expensive and time-consuming. Therefore, the fast development of simulation technologies in the last few decades was key to designing nanoscale devices. Especially for devices that make use of electromagnetic phenomena which feature many parameters and a very high complexity so that it is not possible to predict the behavior theoretically, even if the underlying physics is well understood. One software which became indispensable in the fields of photonics, optoelectronics and nanotechnology is the one developed by Ansys Lumerical. This was also used for the purposes of this thesis.

3.1 Simulation software Ansys Lumerical

Ansys Lumerical's simulation software can be used to construct nanostructures in the shape of rectangles, polygons or rings which can be combined in so-called structure groups in order to define more complex objects like grating couplers. The material database provides values for the refractive index as a function of the wavelength and can be supplemented with custom materials.

One principle type of electromagnetic simulation is the FDTD (Finite Difference Time Domain) simulation, which is a numerical modeling technique for solving Maxwell's equation in time domain. For this simulation, it is also possible to add sources and monitors. The frequency and polarization of the emitted light of every source can be customized, and the type of the source can be chosen. One example is the mode source which ejects one special mode (dependent on the surrounding material) and the gauss source, which has additional parameters like the distance from the waist taking into account the dispersion of the beam. Monitors include the index monitor, to verify the index profile of a setup, and the frequency-domain field and power (DFT) monitor which can collect properties like the transmission T and the E-field magnitude E which both play an important role in the next section. T is the amount of power transmitted through the monitor, normalized to the source power. E is defined by $E = \sqrt{E_x^2 + E_y^2 + E_z^2}$ and also normalized to the source power. The FDTD solver region fixes the region for which the simulation should be conducted, and also whether it is 2D or 3D. The FDTD method discretizes both space and time, allowing for the direct observation of electromagnetic wave propagation, scattering, absorption, and reflection within photonic structures. As a result, the mesh

settings (specifying this discretization) can be specified in the FDTD object as well. To decrease the maximal mesh step that can be used during the simulation for regions where a higher resolution is needed, additional mesh override regions can be defined.

Apart from FDTD the MODE (mode solutions) simulation is an important feature of the simulation software which will also be used in this chapter. It focuses on the eigenmode analysis of waveguides and resonant structures to solve Maxwell's equations in the frequency domain. This allows for the calculation of mode profiles and effective indices of guided modes in optical structures.

3.2 SiN Material Stack

Figure 3.1 shows the typical material setup for the SiN platform. A cladding layer of SiO₂ (green) is covering the optical circuitry (brown) on top of a SiO₂ layer (green) which is grown on a Si substrate (dark brown) which is typically more than 500 μm big so that only the top of it is shown in Figure 3.1.

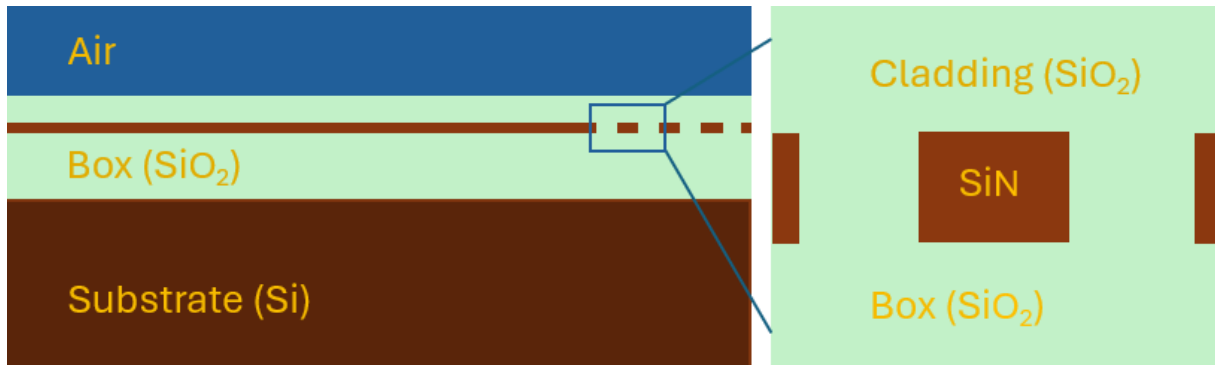


Fig. 3.1 Cross-section of the SiN material stack featuring the following thicknesses:
base: $\approx 500\mu\text{m}$; box: $3.7\mu\text{m}$; circuitry: $0.33\mu\text{m}$; cladding: $0.8\mu\text{m}$

The box- and circuitry-thickness is fixed by the chip manufacturer. The main reason of the box is to prevent the light to couple to the substrate, which has a much higher refractive index of $n \approx 3.5$. Structures such as GCs are fabricated by removing SiN material from areas where it is not needed, employing etching techniques. The primary purpose of the cladding is to protect the circuitry, and its thickness is chosen to match a value that can be easily achieved in our laboratories.

3.3 Finding optimal parameters for a 2D grating coupler

The setup shown in Figure 2.2a will now be used to determine the filling factor FF and the period Λ that optimize coupling efficiency. Combining the bragg Equation 2.3 with the Equation 2.4 and solving for the filling factor FF results in the following expression:

$$FF = \frac{n_c \cdot \sin \theta + \frac{\lambda}{\Lambda} - n_{trench}}{n_{tooth} - n_{trench}} \quad (3.1)$$

λ is set to 1550 nm as this is the wavelength we are interested in, in this work. θ is fixed to -5.65° because the polishing angle of our in-house fiber array is 8° and the final goal of this thesis is the design of a PSGC (compare to Section 2.5). The negative sign is explained in Section 2.4. Next, the values for the effective indices n_c , n_{trench} and n_{tooth} in the direction of the source in the waveguide have to be determined. As the material of the trench is the same as the one above (cladding) and below (box) of the waveguide (SiO_2), the effective index of the tooth is the same as the refractive index of SiO_2 (at $\lambda = 1550$ nm): $n_c = n_{trench} = 1.44$.

The effective index for the tooth n_{tooth} is not the same as the corresponding refractive index of the waveguide material SiN as the surrounding material is different in negative and positive y-direction on a very small length scale ($0.33 \mu\text{m}$). Therefore, the effective index is calculated using the MODE simulation of Ansys Lumerical which was presented above. For the E0 mode (the one guided by the waveguide which is used) which is shown in Figure 3.2a we get $n_{tooth} = 1.68$.

Hence, FF and Λ are the only undetermined parameters of Equation 3.1. Their relationship $FF(\Lambda)$ is shown in Figure 3.2b for reasonable FF between 0.1 and 0.9. Further on, FF is allowed to vary linearly from the initial filling factor $FF_{initial}$ to the final filling factor FF_{final} (remember Figure 2.2a from chapter 2) to implement the linear apodization of the gratings for the self-imaging effect talked about in the theory chapter. FF can be expressed using the initial and the final filling factor as follows:

$$FF = \frac{FF_{initial} + FF_{final}}{2} \quad (3.2)$$

As a next step, simulations in 2D are employed to find the values for $FF_{initial}$, FF_{final} and Λ which optimize the coupling efficiency to the waveguide. If two of these parameters are given, the third one can be uniquely determined due to Equation 3.1 and 3.2. The coupling efficiency is determined measuring the transmission for a DFT monitor covering the cross-

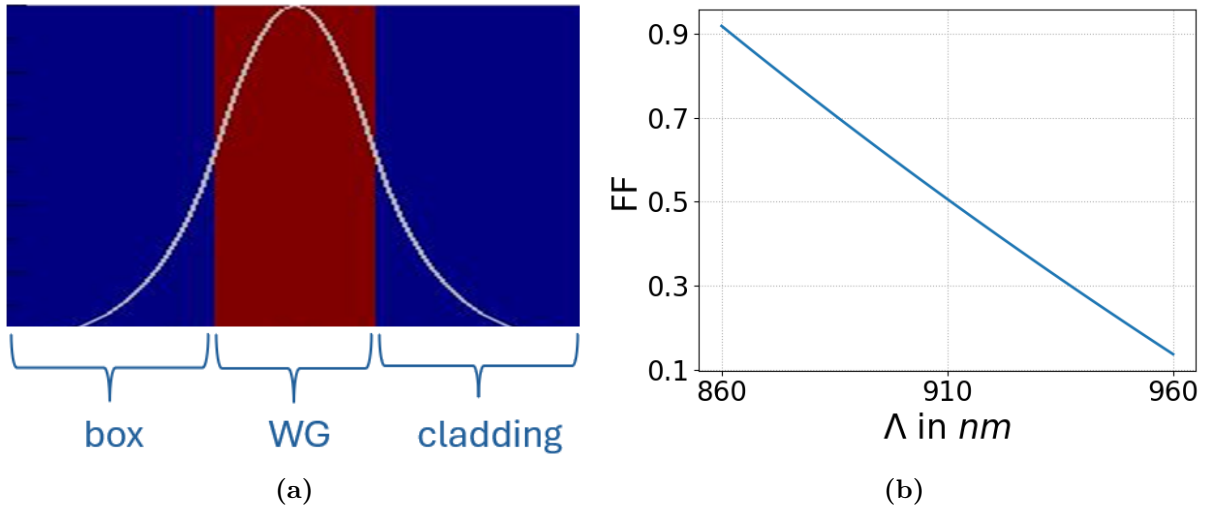


Fig. 3.2 a: TE0 mode of the waveguide (white) with a simulated effective index of $n_{trench} = 1.68$.

b: Filling factor vs period according to Equation 3.1

section of the waveguide for an in-coupling setup. As an example, the transmission of 0.1 corresponds to 10 % coupling efficiency.

3.3.1 Out-coupling simulation configuration

The E-field up-reflection of the out-coupling configuration has to be Gauss-like to ensure efficient coupling to the fiber. In order to achieve this, the initial filling factor has to be maximized as shown in Figure 3.3. This has been theoretically predicted in [10], where it is calculated that the optimal grating strength for a grating coupler to emit a Gaussian beam starts at 0 and increases monotonically with position. The strong oscillations around the running average value are called Fabry-Pérot oscillations. They are caused by the light getting back-reflected into the grating structure due to the index mismatch of the end of the gratings with the waveguide after the gratings. They show that a significant amount of light is still in the waveguide after passing the gratings. Simulations show that it is slightly less than 7 % of the source intensity.

Figure 3.4 points out the region $\Lambda = 890$ nm as being the most promising, as the efficiency for maximal $FF_{initial}$ is the highest. For the red curve which corresponds to the highest shown period of $\Lambda = 910$ nm the maximal initial filling factor of $FF_{initial} = 0.95$ cannot be attained because of 3.1 and 3.2 which can be understood looking again at Figure 3.2b. As this is the same for every other period bigger than 910 nm, they are not shown in Figure 3.4. For smaller periods than $\Lambda = 880$ nm, the overall up-reflection, and therefore the coupling efficiency, further decreases. This is to be expected, as the grating strength diminishes with a higher filling factor, resulting in more light remaining in the waveguide

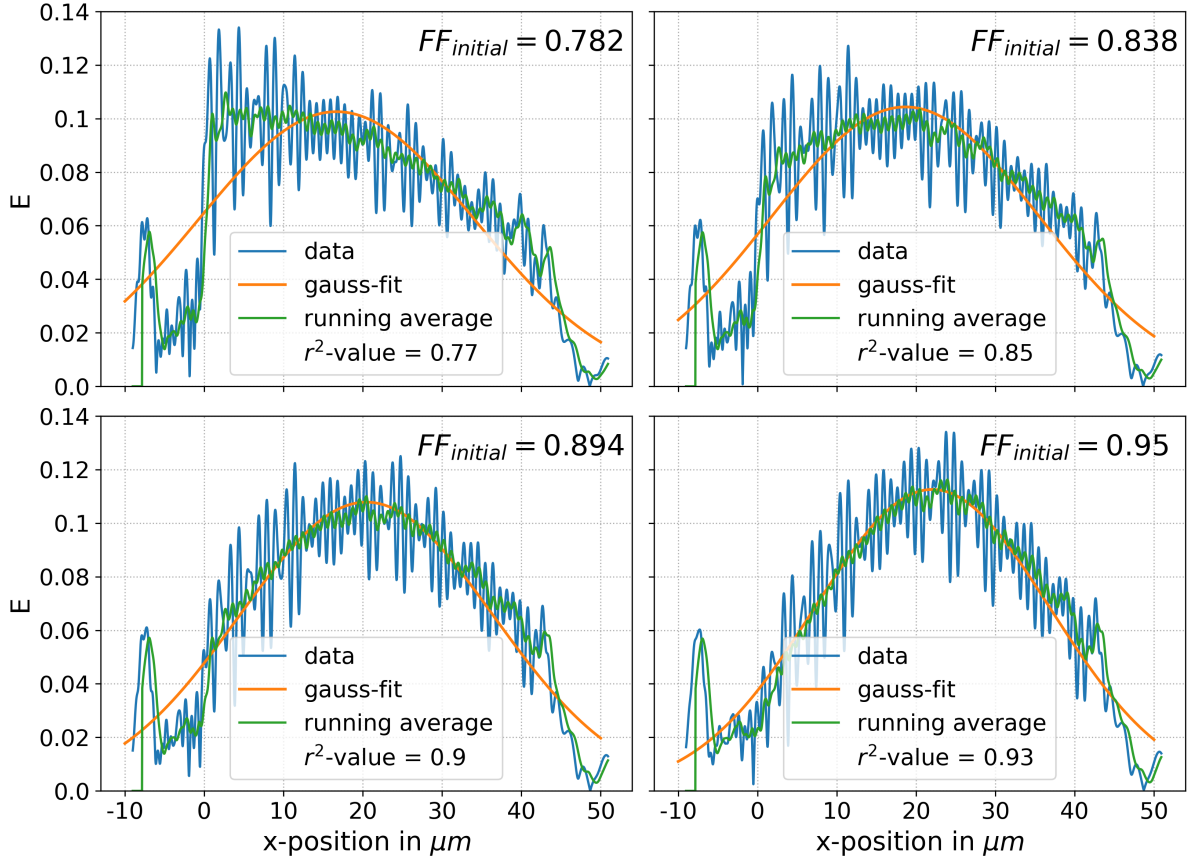


Fig. 3.3 Plotted is the up reflected E-field magnitude E measured by a DFT Monitor which is situated in the air above the grating coupler as a function of the x-location. Λ is fixed at $890\ \mu\text{m}$. The 50 gratings start at $x = 0\ \mu\text{m}$ and end at $x = 44.5\ \mu\text{m}$. The running average plotted in green matches the gauss fit the best for $FF_{initial} = 0.95$ which is also shown with the corresponding r^2 values. The smaller the initial filling factor, the more power is peak-like diffracted at the beginning of the gratings.

instead of being diffracted by the gratings.

Doing a sweep over the period between 886 and 900 nm while keeping the initial filling factor constant at $FF_{initial} = 0.95$ results in the plots of E as a function of the x-position shown in Figure 3.5. Apart from being gauss-shaped like the last plot in 3.3 (the brown one is the last plot of Figure 3.3), they all seem to be quite similar. Looking at the upward reflected power shown in the inset plot in Figure 3.5 one can assume a maximal coupling efficiency at $\lambda \approx 890\ \text{nm}$. Nevertheless, the upward reflected power alone does not take into account that matching the mode of the optical fiber is also necessary for effective coupling. Therefore, for further simulations, the in-coupling setup is used.

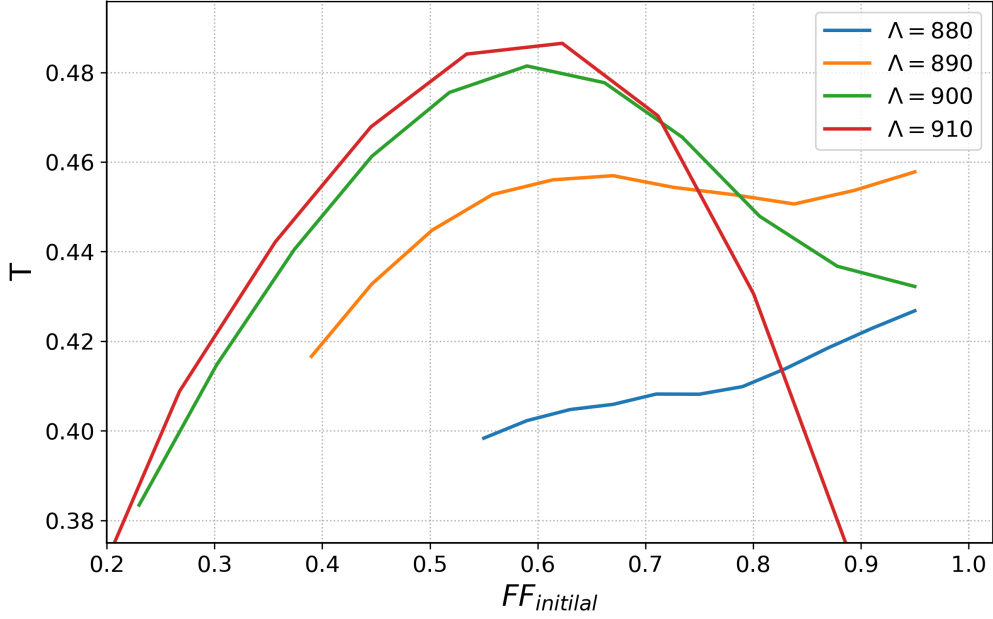


Fig. 3.4 Transmission T as a function of the initial filling factor for four different values for the period Λ .

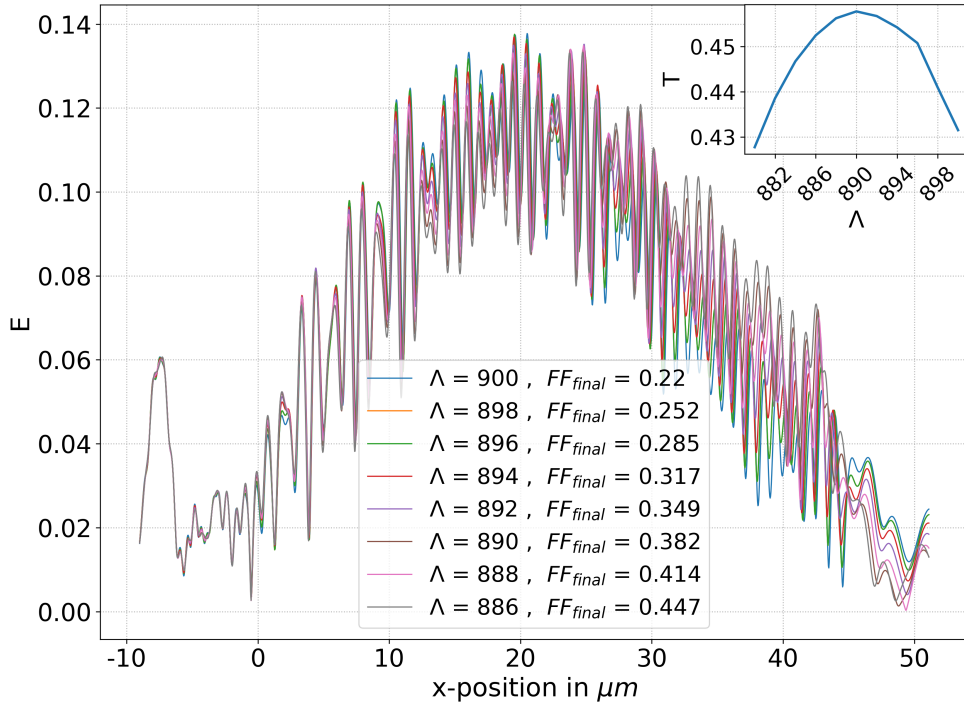


Fig. 3.5 Big plot: Similar to Figure 3.3, E measured by a DFT Monitor which is situated in the air above the grating coupler as a function of the x -location is shown. This is done for eight different values for the period Λ while keeping the initial filling factor fixed at $FF_{initial} = 0.95$. The 50 gratings start at $x = 0 \mu\text{m}$ and end at $x = 44.5 \mu\text{m}$. As expected, all plots exhibit a similar gausslike shape.

Inset plot: transmission as a function of the period Λ at constant $FF_{initial} = 0.95$. The two figures show the same simulation.

3.3.2 In-coupling simulation configuration

The source is positioned in the air over the grating coupler at a diffraction angle of -8.15° , a choice explained at the end of Section 2.5, to simulate the beam leaving the fiber. Two more parameters become relevant: d_x , the distance from the first grating to the place where the beam hits the chip and d_w , the distance from the place where the gaussian beam hits the chip and its waist.

As a next step, Λ , d_x and d_w have to be optimized together. In order to do this, the value range for the two parameters describing the position of the source has - like for the period Λ - to be restricted to a reasonable scope of values.

It is expected that $d_x \approx \frac{50\Lambda}{2} = 22.25 \mu\text{m}$ as this positions the source in the middle of the gratings. However, our setup features a non-disappearing diffraction angle and the mode-field diameter of the gaussian beam grows with the distance from the waist (compare to formula 2.2). This results in a dispersion gap for the part of the beam hitting the beginning of the gratings and the part hitting the end. As a result, the optimal position in x-direction of the source is expected to shift to smaller x . As this is also what was observed during previous simulations conducted within the scope of this thesis (which provide a quantitative guideline of $d_x \approx 18.5 \text{ nm}$), only values for d_x between $17 \mu\text{m}$ and $22 \mu\text{m}$ are considered for further simulations. According to formula 2.2, over the distance $d_w = 190 \mu\text{m}$, the Gaussian beam spreads from a mode-field diameter of $10.4 \mu\text{m}$ to $37.6 \mu\text{m}$, which is 85 % of the grating length (which means that the beam covers the gratings nicely). $300 \mu\text{m}$ was mentioned as an upper boundary for d_w . As a result, values between 90 and 290 are considered.

The simulation to determine the values for Λ , d_x and d_w which maximize coupling efficiency is a nested sweep over all values that come into question based on the preliminary considerations made above. The coupling efficiency for the in-coupling configuration is measured as the transmission T going through the DFT monitor, which covers the cross-section of the waveguide (or taper) directly after the grating structure. The simulation results are shown in Figure 3.6. The maximal coupling efficiency is shown to be 43.8 % ($T = 0.438$) for the values $\Lambda = 892 \text{ nm}$, $d_w = 190 \mu\text{m}$, and $d_x = 19 \mu\text{m}$. As fine-tuning of these parameters doesn't result in an improvement of more than 0.3 %, these are the final optimized values for this section.

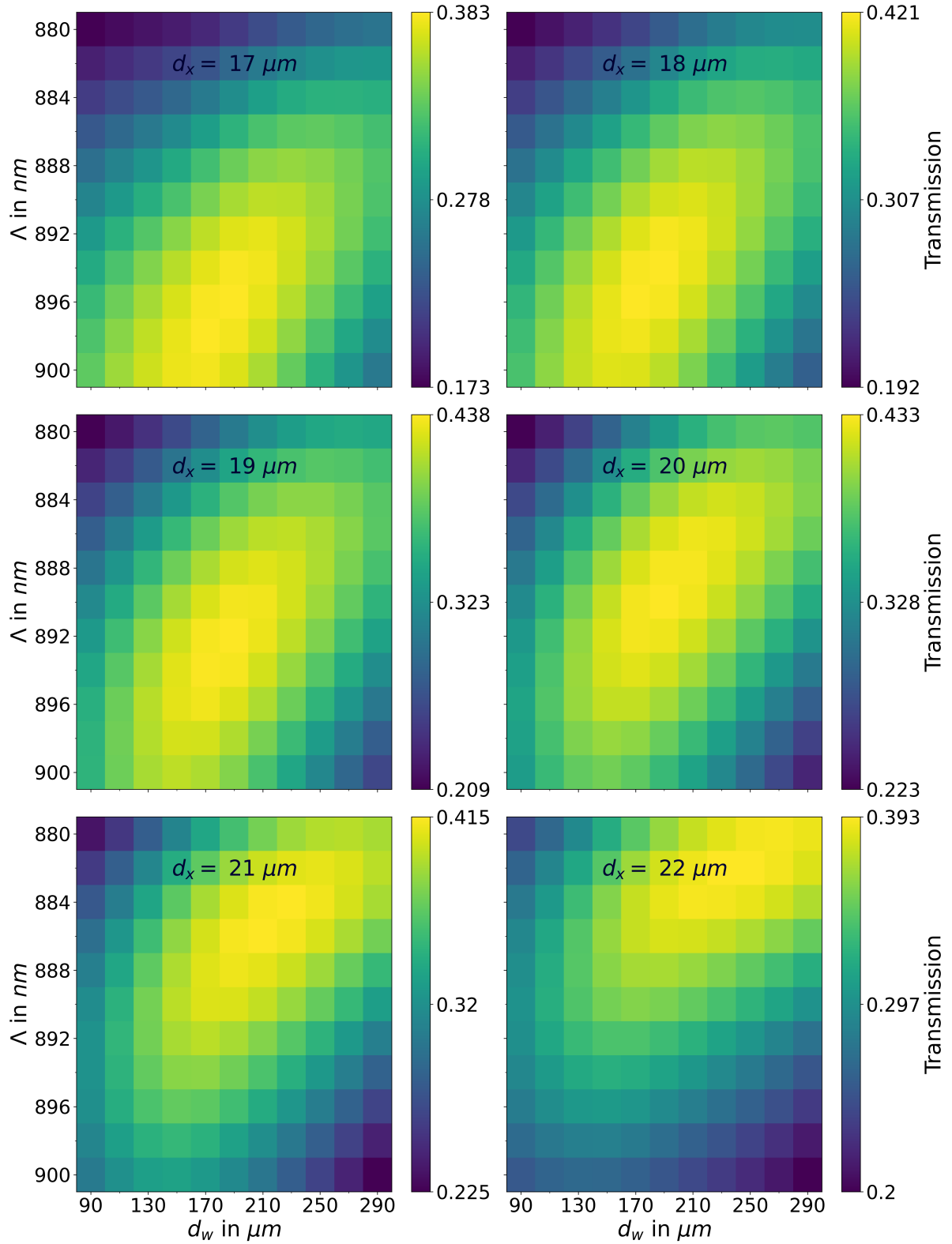


Fig. 3.6 Simulated coupling efficiency as a function of d_w , the distance from the waist of the gauss source, d_x , its position in x-direction and, Λ , the period. The highest efficiency of 0.438 is shown for the plot where $d_x = 19 \mu\text{m}$.

3.4 Optimizing mesh values

The mesh step is the size of the discrete parts into which the simulation region is divided to numerically solve the Maxwell-equations. The smaller it is, the more computationally intensive the simulation becomes, but the higher the accuracy. A good trade-off between accurate results and computational feasibility is needed. The optimal values determined in this section will be employed for the 3D simulations discussed in the next section, where computational feasibility poses a greater challenge. They have also been used for the 2D simulations in order to ensure good comparability.

The concrete mesh parameters to be adjusted are the maximal mesh steps in x-, y- and z-direction (dx , dy and dz) fixed with a mesh override region. The transmission T through a DFT monitor covering the cross-section of the waveguide, measured for a 2D grating coupler in in-coupling configuration, is used as an indicator for the simulation efficiency. The simulation results for this 2D setup are also applicable for the 3D case. Figure 3.7 shows T as a function of dx for different values of dy . Note, that T is systematically lower than the best values in the preceding section as the simulations of this section were conducted before the optimization process was completed.

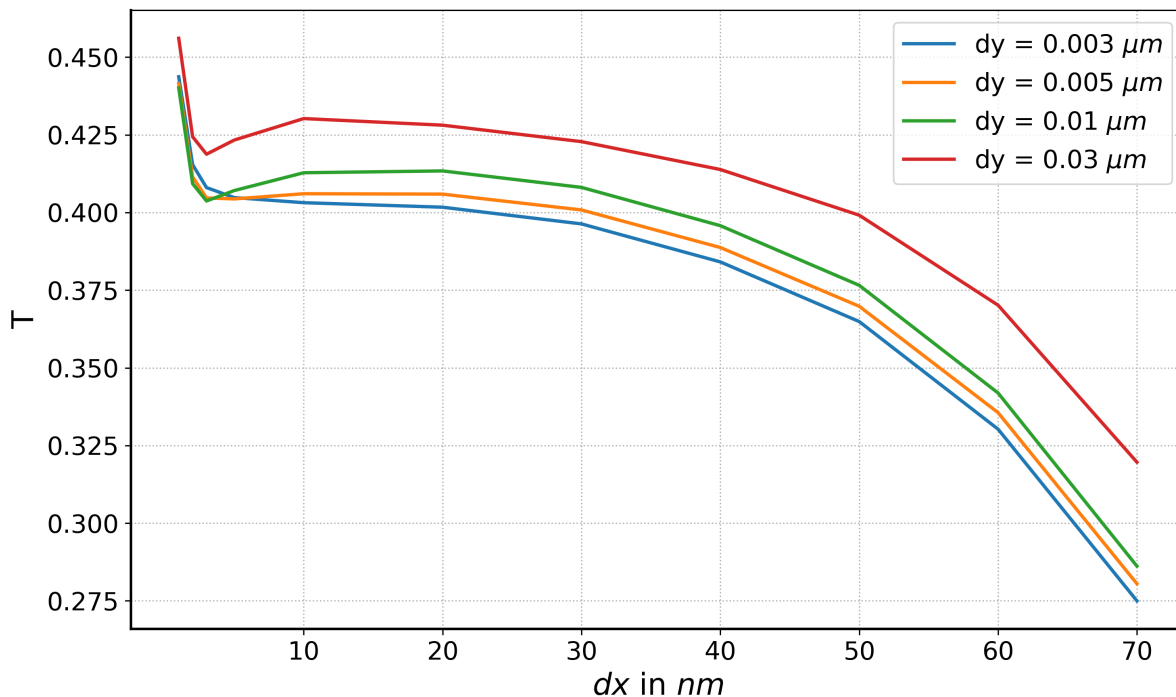


Fig. 3.7 Simulated coupling efficiency vs dx , the maximal mesh step in x-direction.

The transmission drops increasingly for $dx > 30$ nm, and for values $dx < 30$ nm, 3D simulations become too computationally challenging. Further on, the maximal values are

achieved for $dy = 30$ nm. In the case of this simulation, graphs for higher dy stay constant on the maximal values of dy , in general they decrease drastically. Both is only due to computational reasons, which is why it will not be further investigated. As a result, the values chosen for further 3D simulations are $dz = dx = dy = 30$ nm. dz is chosen to match dx as a circular grating lying in the x-z plane features similar setups in x- and z-direction.

The recommendation for the minimal mesh step is a fourth of the minimal feature size (if this is computationally feasible). In the case of the gratings and in x-direction, this is the smallest trench-length of $(1 - 0.95) \cdot \Lambda \approx 45$ nm. Thus, $dx = 10$ nm would be the recommendation, which is too small to be applicable for the 3D sims of the next chapter.

Following the tendency of a strongly improved transmission for a very small maximal mesh step (compare Figure 3.7), we simulate the transmission for the optimal values for $FF_{initial}$, FF_{final} and Λ found in Section 3.3 for $dy = 0.03 \mu\text{m}$ and $dx = 0.0005 \mu\text{m}$. A considerably higher transmission rate of 51.8% has been achieved, suggesting that, in certain scenarios, fabrication might yield better outcomes than simulations predict.

3.5 Continuation in 3D

In order to verify the GC design of the preceding section to be compatible with the use of a PSGC, the angle of the in-coupling source with respect to the gratings has to be adjusted as explained in the previous chapter. Computationally much more demanding 3D simulations were used to find the values for the coupling efficiency to the WG as a function of the polarization angle of the incoming beam, shown in Figure 3.8. In accordance to the theory presented in Section 2.5, the highest value of 17.4% is measured at the polarization angle of -45° , whereas nearly no coupling (0.6%) is measured for the orthogonal polarization of 45° . This demonstrates that coupling to the waveguide is feasible even if the source is not positioned within the plane defined by the GC's symmetry axis and the chip's normal, which is essential for the design of a PSGC. The 17.4% of transmission was measured directly after the gratings. To confine the beam in z-direction as well to a $1 \mu\text{m}$ wide WG, a non-optimized set of two tapers was used as shown in Appendix 2. The additional loss is around 2 dB.

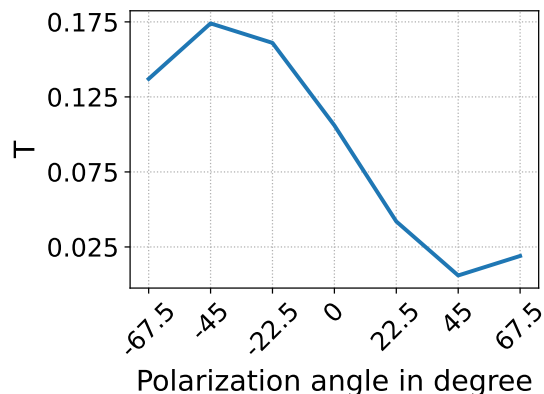


Fig. 3.8 Transmission T as a function of the polarization angle.

4 Outlook

In this thesis, a simulation procedure to find optimal parameters for a 2D GC on the SiN platform was presented while achieving a simulated coupling efficiency of 43.8% for appropriate mesh parameters and 51.8% as a maximal value. These values were achieved for a design which can be used for a PSGC which couples to our in-house fiber array with a polishing angle of 8° . To demonstrate this, a coupling efficiency of 17.4% could be simulated for an in-coupling configuration where the source was rotated 45 degrees out of the plane defined by the GC's symmetry axis and the chip's normal. This corresponds to an additional loss of 4 dB.

Before changing the diffraction angle to $\theta = 5.65^\circ$ some simulations were conducted at $\theta = 8^\circ$. For this setup, the additional loss simulated for the introduction of curved gratings and for changing the source alignment from $\phi = 0^\circ$ to $\phi = 45^\circ$ was less than 1.5 dB each. The cumulative loss of approximately 3 dB is less than the value of 4 dB which is achieved for the $\theta = 5.65^\circ$ setup. Either coupling efficiency is better for bigger diffraction angles, or the coupling efficiency of 17.4% can still be improved.

The loss encountered while further confining the light in transverse direction to couple into the 1-micrometer-wide waveguide is around 2 dB. However, by adapting this non-optimized confinement setup (compare to Appendix 2), it is anticipated that this loss can be drastically reduced.

4.1 Improvement of the 2D GC

There are several ideas to increase the maximal value for the 2D GC presented in Section 3.3.

First, the effective index n_{tooth} for the tooth of the grating structure, which was determined using Lumerical's MODE simulation, changes if more surrounding material is considered. The TE_0 mode for a considered y -span of $3\ \mu\text{m}$ is shown in figure 4.1. The corresponding effective index value is $n_{tooth} \approx 1.697$. The value used for the simulations presented in this thesis is $n_{tooth} = 1.68$. This mismatch changes the values for the filling factor as a function of the period (compare Equation 3.1) about nearly 0.3 dB ($\approx 7\%$), which could have a significant impact on the simulations based on this value. Therefore, an improvement in coupling efficiency might be possible by redoing the simulations presented in Chapter 3

with $n_{tooth} = 1.697$.

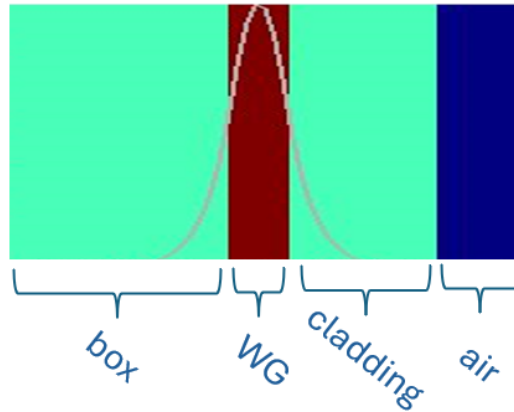


Fig. 4.1 TE0 mode for a 3 μm -region around the waveguide at an x-position of a tooth. The simulated effective index for it is $n_{tooth} \approx 1.697$

Second, the E -field as a function of the direction of the gratings shown in Figure 3.3 and 3.5 features strongly pronounced Fabry-Pérot oscillations, as it was already mentioned. One way to reduce these oscillations is to introduce some gratings with a small filling factor after the GC to weaken the index mismatch [12]. It is possible that this could also improve the grating efficiency, as the approximation of the optimal Gaussian shape would be better.

Third, following the literature [9, 12], 50 was chosen as the number of gratings. This is enough to diffract most of the light out of the waveguide and to implement an apodization to achieve gauss-like up-reflection while staying within the constraints opposed by simulation and manufacture. Still, an increase of more than 0.36 dB (which is more than 9%) in coupling efficiency was simulated for the 2D in-coupling design for an increased number of 70 gratings. As it should in principle be possible to simulate and manufacture devices with a number of gratings higher than 50, this is estimated to be an easy way for further improvement of coupling efficiency.

Fourth, the optimal apodization to achieve gauss-like up-reflection is not linear, which is shown in [10]. Implementing a more precise apodization function could lead to an improvement in coupling efficiency. Nevertheless, this might be difficult, as the optimal linear function already reduces the overlap loss with the fiber mode to 0.5 dB.

4.2 Next steps

The last step to implement a PSGC is to create a structure where scattering elements are placed at the intersections of the two superimposed GCs, like it is demonstrated in Figure 4.2. The angle Ψ is introduced as a further alignment of the WGs is shown to increase coupling efficiency [24, 25]. The shape of these scattering elements plays an important role [10], circles are not the best choice in most of the cases.

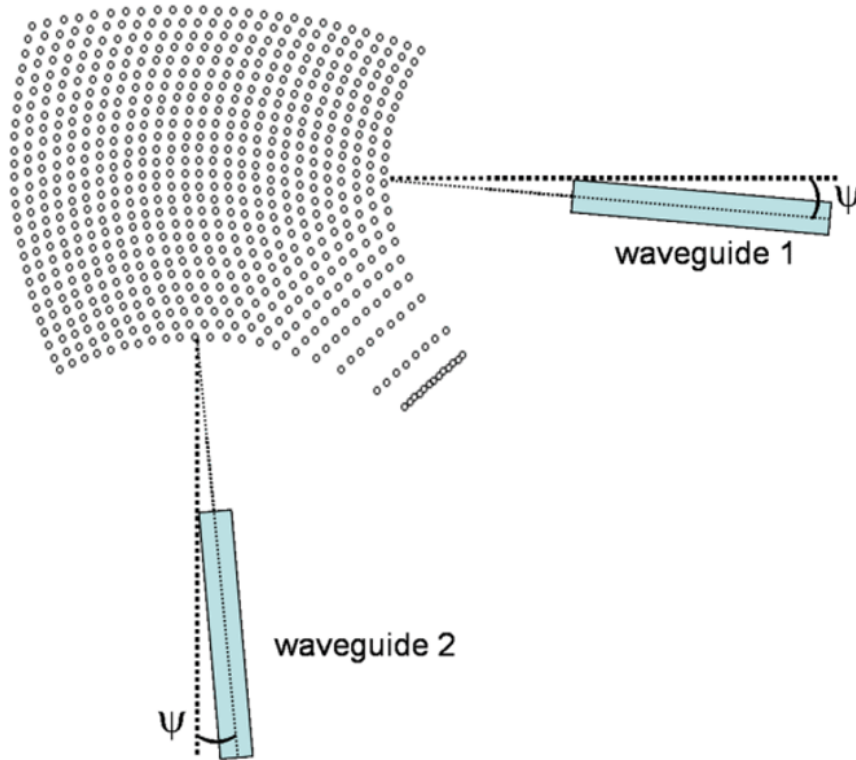


Fig. 4.2 Draft of a PSGC. Adapted from [24].

5 Conclusion

The simulation procedure employed lead to a design of a 2D GC with a maximal coupling efficiency of 51.8 %, which is a very good value for GCs that don't include any backreflector [9]. This design was built in a way so that it can be adopted for the design of a PSGC. Further simulations and theoretical analysis could be used to indicate that PSGCs can be implemented on the SiN platform. Predictions for the coupling efficiency cannot be provided since the last simulation step was not completed, nevertheless, this step was proven to be realizable on other platforms with a coupling loss less than 0.4 dB [24]. This strongly suggests that PSGCs could also serve as valuable devices on the SiN platform, particularly for applications where a 10 dB-loss is still acceptable, given the possibility of high light intensities on SiN.

Bibliography

- [1] L Chang Davanco et al. “Roadmap on integrated quantum photonics”. In: *J. Phys. Photonics* 4.1 (2022), p. 012501.
- [2] Bhavin J Shastri et al. “Photonics for artificial intelligence and neuromorphic computing”. In: *Nature Photonics* 15.2 (2021), pp. 102–114.
- [3] Johannes Feldmann et al. “All-optical spiking neurosynaptic networks with self-learning capabilities”. In: *Nature* 569.7755 (2019), pp. 208–214.
- [4] Yichen Shen et al. “Deep learning with coherent nanophotonic circuits”. In: *Nature photonics* 11.7 (2017), pp. 441–446.
- [5] Jared F Bauters et al. “Ultra-low-loss high-aspect-ratio Si₃N₄ waveguides”. In: *Optics express* 19.4 (2011), pp. 3163–3174.
- [6] Daniel J Blumenthal et al. “Silicon nitride in silicon photonics”. In: *Proceedings of the IEEE* 106.12 (2018), pp. 2209–2231.
- [7] Lukas Chrostowski and Michael Hochberg. *Silicon photonics design: from devices to systems*. Cambridge University Press, 2015.
- [8] Yang Chen et al. “Experimental demonstration of an apodized-imaging chip-fiber grating coupler for Si₃N₄ waveguides”. In: *Optics letters* 42.18 (2017), pp. 3566–3569.
- [9] Emma Lomonte, Francesco Lenzini, and Wolfram HP Pernice. “Efficient self-imaging grating couplers on a lithium-niobate-on-insulator platform at near-visible and telecom wavelengths”. In: *Optics Express* 29.13 (2021), pp. 20205–20216.
- [10] Attila Mekis et al. “A grating-coupler-enabled CMOS photonics platform”. In: *IEEE Journal of Selected Topics in Quantum Electronics* 17.3 (2010), pp. 597–608.
- [11] Ralf Waldhäusl et al. “Efficient coupling into polymer waveguides by gratings”. In: *Applied optics* 36.36 (1997), pp. 9383–9390.
- [12] Emma Lomonte et al. “Scalable and efficient grating couplers on low-index photonic platforms enabled by cryogenic deep silicon etching”. In: *Scientific Reports* 14.1 (2024), p. 4256.
- [13] Yunhong Ding et al. “Fully etched apodized grating coupler on the SOI platform with- 0.58 dB coupling efficiency”. In: *Optics letters* 39.18 (2014), pp. 5348–5350.
- [14] Siddharth Nambiar et al. “High efficiency DBR assisted grating chirp generators for silicon nitride fiber-chip coupling”. In: *Scientific reports* 9.1 (2019), p. 18821.
- [15] Huijuan Zhang et al. “Efficient silicon nitride grating coupler with distributed Bragg reflectors”. In: *Optics express* 22.18 (2014), pp. 21800–21805.

- [16] Dirk Taillaert et al. “A compact two-dimensional grating coupler used as a polarization splitter”. In: *IEEE Photonics Technology Letters* 15.9 (2003), pp. 1249–1251.
- [17] Frederik Van Laere et al. “Focusing polarization diversity grating couplers in silicon-on-insulator”. In: *Journal of Lightwave Technology* 27.5 (2009), pp. 612–618.
- [18] Wim Bogaerts et al. “A polarization-diversity wavelength duplexer circuit in silicon-on-insulator photonic wires”. In: *Optics express* 15.4 (2007), pp. 1567–1578.
- [19] Yongbo Tang, Daoxin Dai, and Sailing He. “Proposal for a grating waveguide serving as both a polarization splitter and an efficient coupler for silicon-on-insulator nanophotonic circuits”. In: *IEEE Photonics Technology Letters* 21.4 (2009), pp. 242–244.
- [20] Matthew Streshinsky et al. “A compact bi-wavelength polarization splitting grating coupler fabricated in a 220 nm SOI platform”. In: *Optics express* 21.25 (2013), pp. 31019–31028.
- [21] Franz Kärtner. *6.974 Fundamentals of Photonics: Quantum Electronics. Spring 2006. Massachusetts Institute of Technology: MIT OpenCourseWare.*
- [22] Riccardo Marchetti et al. “Coupling strategies for silicon photonics integrated chips”. In: *Photonics Research* 7.2 (2019), pp. 201–239.
- [23] Dirk Taillaert. “Grating couplers as interface between optical fibres and nanophotonic waveguides.” In: (2005).
- [24] Frederik Van Laere et al. “Focusing polarization diversity grating couplers in silicon-on-insulator”. In: *Journal of Lightwave Technology* 27.5 (2009), pp. 612–618.
- [25] Frederik Van Laere et al. “Efficient polarization diversity grating couplers in bonded InP-membrane”. In: *IEEE Photonics Technology Letters* 20.4 (2008), pp. 318–320.

Appendix 1

This appendix mathematically proves that for the angles defined in Figure 1, the following relationship applies:

$$\cos \beta = \cos \tilde{\theta}_{45^\circ} \cdot \cos \phi \quad (1)$$

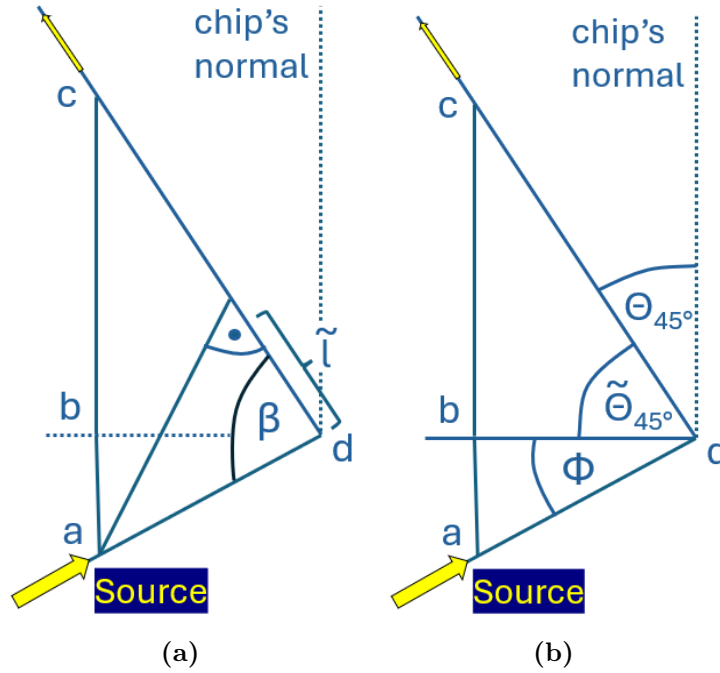


Fig. 1 Both figures represent the identical setup while only different angles are indicated. They show an illustration of an in-coupling setup where the injection axis (defined by the line \overline{cd}) is rotated 45° out of the plane defined by the chip's normal and the direction of the gratings (defined by the line \overline{ad}). The gratings are situated in the plane defined by the points a, d and b, but they are not included in the drawing.

Looking at figure 1b allows us to formulate the following relations:

$$\overline{ab} = \sin(\phi) \cdot \overline{ad}, \quad \overline{cb} = \sin(\tilde{\theta}_{45^\circ}) \cdot \overline{cd}, \quad \text{with } \tilde{\theta}_{45^\circ} := 90^\circ + \theta_{45^\circ} \quad (2)$$

$$\overline{bd} = \cos(\phi) \cdot \overline{ad}, \quad \overline{bd} = \cos(\tilde{\theta}_{45^\circ}) \cdot \overline{cd} \quad (3)$$

$$\overline{ac}^2 = \overline{ab}^2 + \overline{cb}^2 \quad (4)$$

Additionally, through the law of cosines, it is possible to derive a relationship that includes

the angle β :

$$\overline{ac}^2 = \overline{cd}^2 + \overline{ad}^2 - 2\overline{cd} \cdot \overline{ad} \cdot \cos \beta \quad (5)$$

Solving for $\cos \beta$ and simplifying by applying the formulas 2, 3 and 4 can be done as follows:

$$\begin{aligned} \cos \beta &= -\frac{\overline{ac}^2 - \overline{cd}^2 - \overline{ad}^2}{2\overline{cd} \cdot \overline{ad}} \\ &= -\frac{\sin(\phi)^2 \cdot \overline{ad}^2 + \sin(\tilde{\theta}_{45^\circ})^2 \cdot \overline{cd}^2 - \overline{cd}^2 - \overline{ad}^2}{2\overline{cd} \cdot \overline{ad}} \\ &= -\frac{1}{2} \left[\frac{\overline{ad}}{\overline{cd}} (\sin^2 \phi - 1) + \frac{\overline{cd}}{\overline{ad}} (\sin^2 \tilde{\theta}_{45^\circ} - 1) \right] \\ &\stackrel{eq\ 3}{=} -\frac{1}{2} \left[\frac{\overline{bd} \cos \tilde{\theta}_{45^\circ}}{\overline{bd} \cos \phi} (\sin^2 \phi - 1) - \frac{\overline{bd} \cos \phi}{\overline{bd} \cos \tilde{\theta}_{45^\circ}} (\sin^2 \tilde{\theta}_{45^\circ} - 1) \right] \\ &= -\frac{1}{2} \left[\cos \tilde{\theta}_{45^\circ} (-\cos \phi) + \cos \phi (-\cos \tilde{\theta}_{45^\circ}) \right] \\ &= \cos \tilde{\theta}_{45^\circ} \cdot \cos \phi \end{aligned} \quad (6)$$

qed.

Appendix 2

Figure 2 shows the setup used for the 3D simulations of section 3.5:

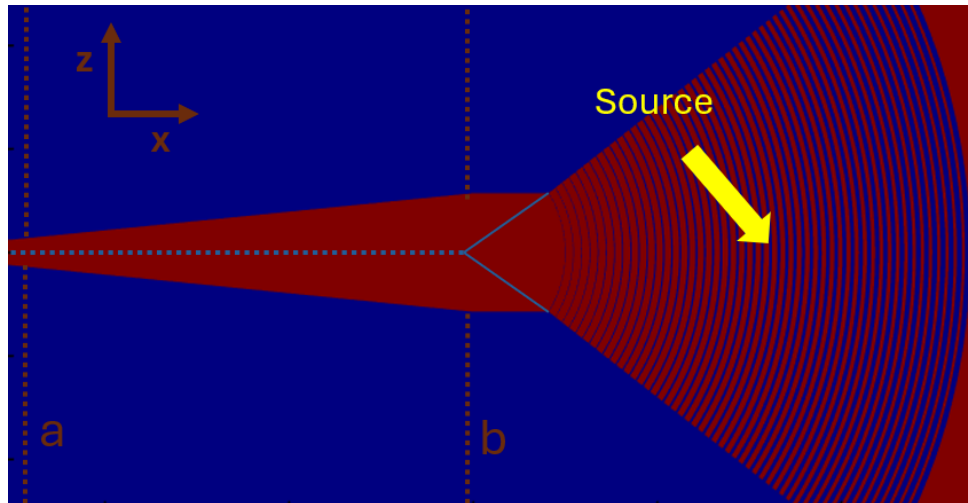


Fig. 2 Coupling efficiency measured at x-position a is 17.4% and at position b 10.5%. The taper width at b is approximately 11 μm and at a (where the second taper from 2.5 μm to 1 μm , for which low loss is expected, starts) 2.5 μm .

Appendix 3

Important files and information about the simulations on which this thesis is based can be found on the following Git-repository:

[BA-simulations](#)

Acknowledgements

At the very end of this thesis, I would like to thank all those individuals, without whom this work would not have been possible in this form.

First of all many thanks to Liam for his never ending "shoot!" when being asked a question, even though I was never the only person having this idea and for inspiringly leading me through the project.

Thanks to Wolfram for giving me the chance to immerse myself into a research group I not only experienced as professional and diverse but also as guided by a warm-hearted atmosphere.

I would like to thank everyone of this group for shaping my first contact with the daily live of doing research. Thanks for bringing a second screen, thanks for helping me to configure my network connection, thanks for sharing experiences, ideas and snacks and thanks for taking the time when needed and not only when available.

I would also like to thank Prof. Oberthaler, who kindly agreed to take the role of the second referee.

Special thanks to Ole for the most valuable feedback regarding this work.

Many thanks to Moritz for accelerating the development of my idea of how a good thesis should look like and to all other friends and fellow students like Andreas, Jakob or Timo, who shared thoughts over my thesis.

Thanks to ChatGPT-4 for tirelessly providing me with feedback on my English language skills.

Last but not least, I would like to thank my parents, without whom, I could have never immersed myself into physics like I did and whose mental support is always easily bridging the 292 km from home!

Declaration of Academic Integrity

I hereby declare that I have authored this work independently and have not used any sources or aids other than those indicated.

A handwritten signature in blue ink, appearing to read 'T. Prall', is positioned below the declaration text.

March 26, 2024